Products of Thymine Oxygenation by a Non-heme Oxygenation Model, $Fe^{II}(MeCN)_6^{2+}$–Ac_2O–H_2O_2, and the Transition State Model between Oxoiron and Thymine

Shigeki KOBAYASHI,*[,a] Akihiko TAKAGI,[a] Toshiyuki CHIKUMA,[a] Osamu TAMURA,[b] Eiichi KOTANI,[b] and Takao KATASE[c]

[a] *Division of Analytical Chemistry of Medicines, Showa Pharmaceutical University;* [b] *Organic Chemistry, Showa Pharmaceutical University; 3–3165 Higashi-tamagawagakuen, Machida, Tokyo 194–8543, Japan: and* [c] *College of Bioresource Sciences, Nihon University; 1866 Kameino, Fujisawa, Kanagawa 252–8510, Japan.*

Received June 27, 2009; accepted March 2, 2010; published online March 11, 2010

Oxidative thymine damage was investigated using a new non-heme oxygenation model, $Fe(MeCN)_6^{2+}$–H_2O_2–Ac_2O, based on high-spin $Fe(MeCN)_6^{2+}$ in a non-aqueous solution, Ac_2O–MeCN. Thymine and 1,3-dimethylthymine oxidized by the system gave the corresponding *trans*-thymine glycol derivatives in good yield. Thymineglycol is equivalent to an oxidative product as a measure of oxidative DNA damage in living cells. It is suggested that the activation of $Fe(MeCN)_6^{2+}$–H_2O_2–Ac_2O in Ac_2O–MeCN forms the oxoiron $O=Fe^{IV}(AcO)(MeCN)_4^+$ as an active species *via* a hetelolytic two-electron mechanism, not a Haber–Weiss–Fenton-type reaction with a one-electron process by treatment with a radical scavenger. In addition, we also demonstrated the transition state (TS) for the interaction between thymine and $O=Fe^{IV}(AcO)(MeCN)_4^+$ in the triplet spin (spin multiplicity; M=3). This model of oxidative thymine damage may provide new insight into the oxidative mechanism of thymine glycol production in non-aqueous reactions of thymine.

Key words iron(II) hexakisacetonitrile; oxoiron; DNA damage; thymine glycol; transition state

The radical abstractions by the reaction of DNA and proteins with reactive species such as active H_2O_2, $HO^{\cdot}$, $HOO^{\cdot}$ and superoxide anion ($O_2^{-\cdot}$) radicals present in living cells are caused by oxidative DNA damage implicated in neurodegeneration, inflammation, cancer, and aging.[1—3] In particular, HO radical has been shown to be generated in aqueous solutions by ionizing radiation,[4,5] UV irradiation,[6] and Fenton-catalyzed Haber–Weiss-type reactions (Fenton reaction).[7,8] In order to elucidate the mechanism and oxidative products, therefore, Fenton reactions with DNA and DNA bases, pirimidines and purines, have been powerfully carried out by many scientists using Fenton-like biomimetic oxygenation models, such as *m*-chloroperbenzoic acid (MCPBA),[9] Fe^{3+}–ethylenediaminetetraacetic acid (EDTA)–H_2O_2,[10] Fe^{3+}–nitrilotriacetic acid (NTA)–H_2O_2,[11] Fe^{3+}–EDTA-ascorbic acid–O_2,[12] and OsO_4.[13]

The major reactive species of oxygenation systems is the HO radical, which is caused by hydrogen abstraction, addition, and electron transfer. On the other hand, oxoirons ($Fe^{IV}=O$ or $Fe^{V}=O$)[14] are known to be provided in reactions catalyzed by $Fe^{2+\text{ or }3+}$ in the presence of H_2O_2 solution. In particular, oxoiron species are found in the catalytic cycles of cytochrome P450 (CYP). The CYP model has been used in mechanistic studies to develop oxoiron complexes, and for oxygenation. A review recently reported the reactivity of oxoiron in chemical and biological oxygenation.[15]

Thymine glycol (5,6-dihydroxy-5,6-dihydrothymine) is produced by oxidative damage of DNA thymine and has been detected in the urine of cancer patients[16]; it is an important marker of cancer. Thymine glycol has been used to elucidate the mechanism causing cancer based on the correlation between its production and oxidative damage to DNA. Detection of urinary thymine glycol has been suggested as a measure of oxidative damage to DNA in humans and animals.[1,2,7] The release of thymine glycol and thymidine glycol from damaged DNA has been shown to take place *via* DNA repair by thymine glycol glycosylase and excision repair, respectively[17,18]; however, the mechanisms by which thymine glycol is formed from OH radicals in the oxidative damage of DNA are not fully understood.

Previously, we reported a new highly effective oxygenation system, $Fe^{II}(MeCN)_6^{2+}$–H_2O_2–Ac_2O, in a hydrophobic medium, such as a dry Ac_2O–MeCN solution.[19—22] In this paper, we report the efficient oxidative damage of thymine using $Fe^{II}(MeCN)_6^{2+}$–H_2O_2–Ac_2O, based on a high spin iron(II) complex, $Fe^{II}(MeCN)_6^{2+}$ (M=5, spin multiplicity), in a dry Ac_2O–MeCN solution. The oxygenation of pyrimidine bases, thymine, and *N*,*N*-dimethyl thymine with the $Fe^{II}(MeCN)_6^{2+}$–H_2O_2–Ac_2O system efficiently produced *trans*-thymine glycol derivatives (major products). We think that *trans*-thymine glycol derivatives form *via* a thymine–O–Fe generated by $Fe^{IV}=O$ acetonitrile complex not *via* the OH radical because thymine treated with a radical scavenger in the $Fe^{II}(MeCN)_6^{2+}$–H_2O_2–Ac_2O system also yielded *trans*-thymine glycol derivatives. Interestingly, the production of parabanic acid has not been reported by thymine oxygenation with Fenton systems. This suggests that the system of oxygenation is new, consisting of a dioxygenase-like model *in vitro* that plays an important role in determining the mechanism of thymine glycol transformation in the oxidative damage of thymine. It is indicated that active species of $Fe(MeCN)_6^{2+}$ using Fe^{II} in a hydrophobic medium or hydrophobic reaction field containing Ac_2O in MeCN solution favor a high valency Fe=O rather than an OH radical. Ac_2O (=activator) plays an important role as a driving force to complete the reaction pathway, $Fe^{II}\cdots OOH \rightarrow Fe^{II}\cdots OOAc \rightarrow Fe^{IV}=O+AcO^-$.

Results

Thymine Oxygenation Previously, we demonstrated

* To whom correspondence should be addressed. e-mail: kobayasi@ac.shoyaku.ac.jp

high redox potential (E_0) and oxidation using an iron(II) hexakisacetonitrile perchlorate ($Fe(MeCN)_6(ClO_4)_2$) complex prepared from iron(II) hexakishydrate perchlorate by treatment with Ac_2O in a dry MeCN solution.[19,21] We found that the acetonitrile solvated ($Fe(MeCN)_6^{2+}$) complex is able to cleave the heterolytic O–O bond of H_2O_2 in a non-aqueous Ac_2O–MeCN solution. To elucidate the mechanism of oxidative DNA damage in non-aqueous media, oxidative thymine damage was investigated.

Oxidative change of thymine **1a** in a $Fe^{II}(MeCN)_6^{2+}$–H_2O_2–Ac_2O system under the optimum molar ratio of $Fe(MeCN)_6^{2+}$, H_2O_2, and thymine in MeCN at 20—30 °C provided the corresponding *trans*-1-acetyl-5,6-diacetoxy-5,6-dehydrothymine (**4a**), mp 131—132 °C, as a major product in 12% (mol%) yield, *trans*-5,6-dihydroxy-5,6-dehydrothymine (**2**), mp 221—224 °C, as a minor product in 3% (mol%) yield, and the structure unknown products. These products, **2** and **4a**, were isolated and purified using silica gel column chromatography and their chemical structures were deduced by analyzing their IR, ^{1}H-, ^{13}C-NMR, hetero-nuclear single quantum coherence (HSQC) NMR, and MS spectra. Protons of C(6)-H and amido proton (–CON(3)HCO–) in **4a** were observed at δ 7.43 (1H, s) and 8.01 (1H, br) in $CDCl_3$ solution, respectively. The amido proton disappeared with the addition of D_2O. The correlation peak between the low-field proton at δ 7.43 and the carbon at δ 75.4 was observed by HSQC and supports the structure of **4a**. The CH_3 protons of three acetyl groups at C(5), C(6), and N(3) observed at δ 2.06, 2.10, and 2.58, respectively, are consistent with the structure of **4a**. Compound **4a** is equal to *trans*-thymine glycol **2**.

When the amount of $Fe^{II}(MeCN)_6^{2+}$ was reduced from 1 to 1/10 eq, **4a** was not obtained at the TLC level. To understand the interaction between $Fe(MeCN)_6^{2+/3+}$ and thymine **1a** in a non-aqueous MeCN solution, the binding ratio between Fe^{2+} and thymine was determined by the molar ratio method using UV/Vis spectrometry (see Fig. 3).

1,3-Dimethylthymine Oxygenation To elucidate the mechanism of oxidative damage to thymine, 1,3-dimethylthymine (**1b**) was oxygenated with the $Fe^{II}(MeCN)_6^{2+}$–H_2O_2–Ac_2O system in non-aqueous Ac_2O–MeCN as described above. The oxygenation of **1b** yielded oxidative products, such as *trans*-5-hydroxy-6-acetoxy-1,3-dimethyl-5,6-dehydrothymine (**5a**; *Rf*=0.61, 2.4% MeOH/$CHCl_3$) as major products and *N*,*N*′-dimethylparabanic acid (**6b**) in yields of 10 and 1% (mol%), respectively. *trans*-Thymine glycol derivative **5a** was afforded in higher yield than isomer **5b**, *trans*-5-acetoxy-6-hydroxy-1,3-dimethyl-5,6-dehydrothymine (*Rf*=0.23, 2.4% MeOH/$CHCl_3$), in yields of 5%. Compound **6b** was also afforded by treatment of *N*,*N*-dimethyluracil and caffeine with the $Fe^{II}(MeCN)_6^{2+}$–H_2O_2–Ac_2O system (not shown data). Although **6b** is a minor oxidative product, its preparation bears little similarity to that of thymine glycol.

NMR simulations suggested that the C(6) proton signals of **5a** and **5b** are observed as δ 6.36 and δ 6.13, respectively and the C(6) carbon siganals of **5a** and **5b** are recorded as δ 90.2 and δ 83.5, respectively. We estimated binding positions of OH and OAc groups in **5a** and **5b** using simulation results. Indeed, the actual C(6) proton signal of **5a** was δ 5.8, and the actual C(6) proton signal of **5b** was δ 5.4. The observed C(6) carbon signal of **5a** was δ 90.1, and the actual C(6) carbon signal of **5b** was δ 80.9.

Generally, oxygenation of thymine and *N*,*N*-dimethylthymine in this system occurs even if $Fe(MeCN)_6^{2+}$ changes to $Fe(MeCN)_6^{3+}$.

Stereochemistry of the Thymine Glycol Derivative (4a) The stereochemistry of thymine glycol derivative **4a** was determined by comparison with *cis*-thymine glycol (**3**) prepared by $KMnO_4$ oxidation of thymine at pH 7.1.[23—25] When **3** was reacted with 4-*N*,*N*-dimethylaminopyridine (DMAP) in Ac_2O, *cis*-1-acetyl-5,6-diacetoxy-5,6-dehydrothymine (**4b**) was obtained. Therefore, the stereochemistry of **4a** (*Rf*=0.47, 9% AcOEt/$CHCl_3$) was assigned a *trans* configuration based on a comparison with **4b** (*Rf*=0.35, 9% AcOEt/$CHCl_3$). The stereochemistry of **2** was assigned a *trans* configuration through comparison with **3** (Fig. 2).

UV/Vis Studies If a $Fe^{2+/3+}$ ion is bound to thymine, the UV/Vis absorbance of $Fe(MeCN)_6^{2+/3+}$ must change. The change in absorbance was analyzed by the molar ratio method. A wavelength of 340 nm was used based on the π–π^* absorption of $Fe(MeCN)_6^{2+/3+}$ (fixed concentration: 1×10^{-4} M) in the solvated $Fe(MeCN)_6^{2+/3+}$–thymine complex. The results of the molar ratio method are shown in Fig. 3, which shows a plot of the absorbance (at λ_{max}=340 nm) against the [thymine]/[Fe^{3+}] ratio obtained by UV/Vis measurements. The fact that the [thymine]/[Fe^{3+}] ratio equals 1 suggests that thymine binds with Fe^{3+} (or Fe^{2+}) ions at a 1 : 1 molar ratio; therefore, direct interaction would occur between $Fe(MeCN)_6^{3+}$ (or $Fe(MeCN)_6^{2+}$) and thymine, and the chemical equibrium would move to the right-hand side of Eq. 1.

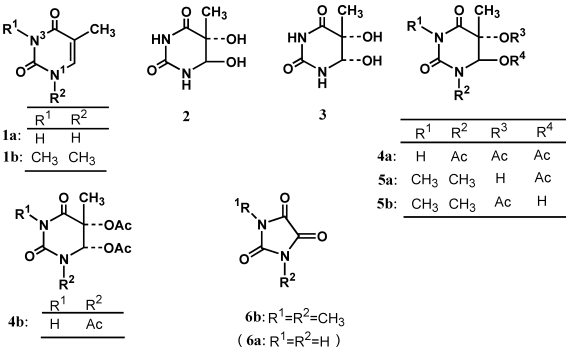

Fig. 1. Oxidative Products of Thymine with $Fe^{II}(CH_3CN)_6^{2+}$–H_2O_2–Ac_2O System

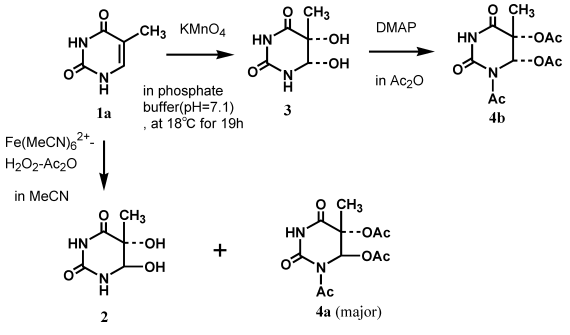

Fig. 2. Determination of Stereochemistry (*cis*- or *trans*-) of Thymine Glycol Derivative **4a**

$$\text{thymine} + Fe^{3+} \rightleftarrows [\text{thymine}–Fe^{3+}] \quad (1)$$

Active Oxoiron O=Fe^{IV}(OAc)$^+$ Species Ligand OH_2 in the $Fe(OH_2)_6^{2+}$ complex is easily substituted with MeCN in the presence of Ac_2O in MeCN. In the case of activation by the addition of H_2O_2, the H_2O_2 ligand easily replaces MeCN in a high-spin $Fe^{II}(MeCN)_6^{2+}$ complex, and the $Fe^{II}(MeCN)_m(O–OH)^+$ intermediate is formed. The $Fe^{II}(MeCN)_m(O–OH)^+$ intermediate forms a $Fe^{II}(MeCN)_m(O–OAc)^+$ complex on treatment with Ac_2O, and the complex changes to the active oxoiron, $O=Fe^{IV}(OAc)(MeCN)_m^+$, *via* the cleavage of a heterolytic O–O bond.[19,22] In a previous study, we suggested that the $Fe^{II}(O–OAc)(AcOH)(MeCN)_4^+$ complex **7** accelerates the molecular exchange of MeCN with AcOH on $Fe^{II}(O–OH)(MeCN)_6^{2+}$ by cleavage of the O–O bond due to intermolecular hydrogen bond interaction (Fig. 4).[19—22] To elucidate the mechanism behind the formation of the thymine glycol derivative **4a** or **5a**, we computed the structure and electron states of the active species **9** and **10** by the density functional theory (DFT) method using a LCAVP(D) basis set and by the semiempirical method using the UPM3(D) hamiltonian. The DFT calculation revealed the possible activation mechanism from the octahedral $Fe^{II}(MeCN)_6^{2+}$ complex to oxoiron ($Fe^{IV}=O^{2+}$) on treatment with H_2O_2 in an Ac_2O–MeCN solution. Here, we present the geometry and electron state of the optimized $O=Fe^{IV}(OAc)(MeCN)_n^+$.

Figure 5 shows the structure of the active oxoiron species of both $O=Fe^{IV}(OAc)(MeCN)_4$ **9** and **10** as shown in Fig. 4. For the *cis* complex **12a**, the spin multiplicity of the ground state is found to be a triplet (M=3), and the lengths ($r_{Fe–O}$) of $Fe^{IV}=O$ and Fe^{IV}–OAc are 1.624 and 1.870 Å, respectively, which were obtained using the UB3LYP/LACVP(D) method. The $r_{Fe–O}$ distances of the *trans* complex **13a** (M=3) are 1.656 and 1.909 Å, longer than those of *cis* **12a**. Although the total energy (E) in the ground state of **12a** is lower by 11.9 kcal/mol than that of **13a**, the energy difference is very small. Detailed exploration revealed that the AcO ligand of **13b** is stable in $\angle N^1$–Fe–O^2–C^3=44.3° on the *yz* plane. From an energy viewpoint, **13b** is more stable than **13a** due to the resonance effect of the AcO ligand in the intramolecule. The Fe=O bond length ($r_{Fe–O}$) in **13b** is 1.650 Å, as listed in Table 1. This value is similar to that of the oxoiron(IV) intermediate (=1.65—1.68 Å).[26] The energy of the stable isomer **13b** is characterized by the stretched conformation of the AcO ligand. In addition, the highest occupied molecular orbital (HOMO) energy (ε_{homo}) of **13b** is −8.84 eV higher than the values of −10.57 and −10.36 eV for **12a** and **13a**, respectively. Moreover, the lowest unoccupied molecular orbital (LUMO) energy (ε_{lumo}) of **13b** is also −5.64 eV, lower than **12a** and **13a**. In the case of the active species **13b**, a stronger oxygenation force than that of **12a** is expected because the redox potential (E_0) is given approximately by relation $E_0 \propto \varepsilon_{homo}$.[27] Indeed, it was found that the oxoiron of **9** is extracted by oxidizing a proton from the Me-group of the AcO ligand and transferring to **11**, as illustrated in Fig. 4. We think that $O=Fe^{IV}(OAc)(MeCN)_4$ provides strong oxygenation of the structure of **13b**.

The structures of the trans forms **13c** and **d** were obtained by the semiemperical UPM3(D) method. The AcO ligand of the *trans* **13c** is in the *yz* plane. The dihedral angle $\angle N^1$–Fe–O^2–C^3 of **13c** is 0.32° along the *x* axis. The calculated value of the Fe=O bond length is 1.686 Å; however, the AcO ligand of the other stable conformer **13d** is twisted by 47.4° along the *x* axis. The stretched structure of **13d** is similar to that of **13b** obtained by the UB3LYP/LACVP(D) method. The conformer **10** produced by the claw-like ligand

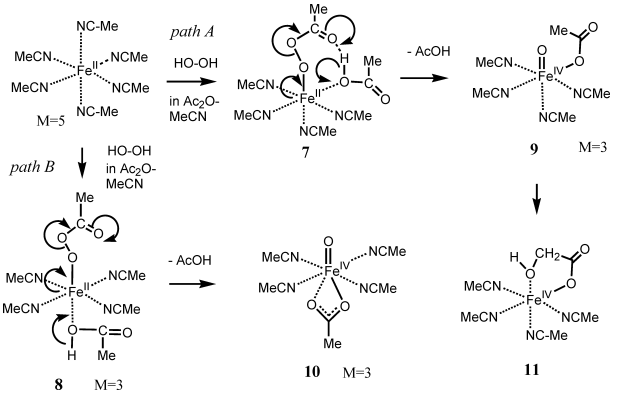

Fig. 4. Two Possible Paths for Production of the Hypervalent Oxoiron Complex, $O=Fe^{IV}(OAc)(MeCN)_4^+$

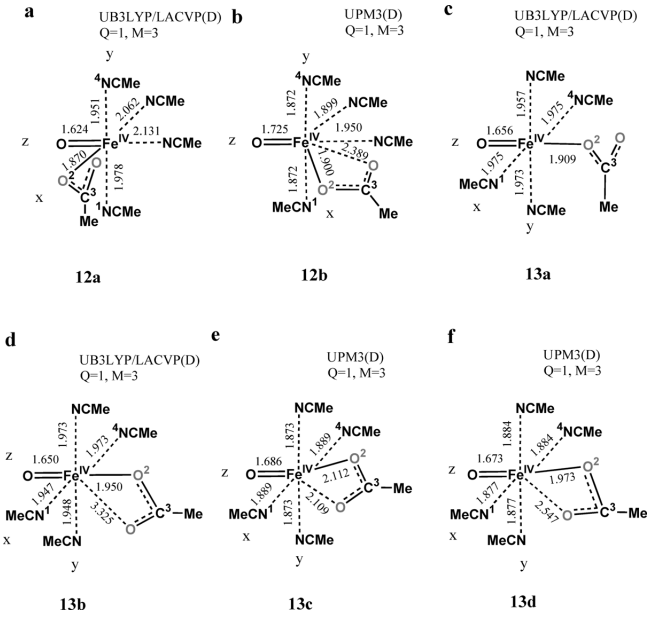

Fig. 5. Structure of Two Possible Hypervalent Oxoiron Complexes, $O=Fe^{IV}(OAc)(MeCN)_4^+$, at UB3LYP/LACVP(D) or UPM3(D) Level

Lengths and dihedral angles are in angstroms (Å) and degree (°), respectively. Energies are given in au or eV units and correspond to the triple state (M=3). The charge (Q) is +1 in all cases.

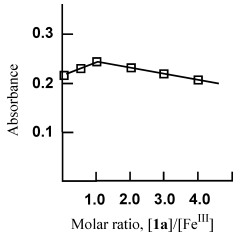

Fig. 3. Continuous Variation Plot of Thymine with $Fe^{III}(MeCN)_6^{3+}$ at λ=314 nm

The concentration ratios of [**1a**]/[Fe^{3+}] are equal to=0.0, 0.25, 1.0, 2.0, 3.0, and 4.0. Concentration of Fe^{3+} is 1.0×10^{-4} M at 32 °C in MeCN.

Table 1. Parameters of Energy, Geometry, and Frequency for Optimized Active Species, $O=Fe^{IV}(AcO)(MeCN)_4^{+}$ [a)]

	cis		*trans*			
	12a UB3LYP/ LACVP(D)	**12b** UPM3(D)	**13a** UB3LYP/ LACVP(D)	**13b** UB3LYP/ LACVP(D)	**13c** UPM3(D)	**13d** UPM3(D)
r(Fe=O) (Å)	1.624	1.725	1.656	1.650	1.686	1.673
r(Fe–O^2Ac) (Å)	1.870	1.900	1.909	1.950	2.112	1.973
r(Fe–OAc) (Å)	3.272	2.389	3.655	3.325	2.109	2.547
r(Fe–N^1) (Å)	1.978	1.872	1.975	1.947	1.889	1.877
r(Fe–N^4) (Å)	1.951	1.872	1.973	1.973	1.889	1.884
ν(Fe=O) cm^{-1}	847.1	740.2	779.4	827.8	980.5	1065.3
ν(Fe–OAc) cm^{-1}	939.4	901.7	609.9	654.2	694.3	740.9
ν(FeOC=O) cm^{-1}	1732.6	1813.1	1760.8	1722.0	1635.9	1841.4
$\angle N^1$–Fe–O^2–C^3 (°)	+142.3	−179.3	+8.7	+44.3	+0.32	+47.4
ε_{homo} (eV)	−10.566	−12.462	−10.363	−8.840	−12.106	−12.634
ε_{lumo} (eV)	−5.037	−3.009	−5.335	−5.636	−2.743	−2.761
Energy	−957.981 [b)]	−9.689 [c)]	−957.962 [b)]	−958.003 [b)]	−10.154 [c)]	−10.096 [c)]

a) Parameters of $O=Fe(AcO)(MeCN)_4^{+}$ in the triple state (M=3). The change (Q) is +1. *b*) Total energies are given in au units. *c*) Heat of formation is given in eV units. Standard thermodynamic quantities are the vlues at 298.15 K and 1.00 atm in all cases.

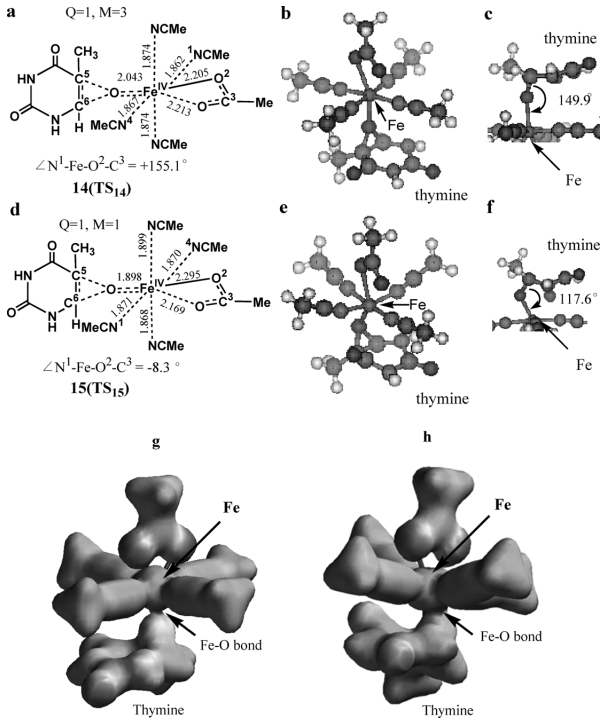

Fig. 6. Optimized Energy, Geometries, and Potential Map of the Imaginary Modes of Two Possible Transition States for Oxygenation of Thymine with $O=Fe^{IV}(AcO)(MeCN)_4^{+}$ Complex Corresponding to the Triplet (M=3) (a—c, and g) and Singlet (M=1) (d—f, and h) States

[a] Geometries and ball and stick presentations of **14** (TS_{14}) (a, b) and **15** (TS_{15}) (d, e). [b] Angle of ∠Fe–O–C(6) (thymine) (c, f). [c] Potential map of the bond density (g, h).

of AcO^- along the x axis is energetically more stable than **9** in Fig. 4. Next, we show the results of the reaction between **13c** and thymine with the $Fe^{II}(MeCN)_6^{2+}$–H_2O_2–Ac_2O system.

Transition State of Thymine–O=Fe^{IV}(OAc)$(MeCN)_4^{+}$ To elucidate the mechanism for effective oxygenation of the active species **13c** with thymine, we simulated the activation energy (E_{TS}) and transition state between **13c** and thymine. The transition state (TS) was designed in accordance with the ground state of thymine–**13c** using the transition state optimization function of the Spartan program. The two TSs, TS_{14} and TS_{15}, between **13c** and T in the ground state are the possible structures with a triplet state (M=3) or singlet state (M=1) at electronic charge $Q=+1$, respectively. The TS optimization of **14** (TS_{14}) and **15** (TS_{15}) was performed by the UPM3(D) method and the results obtained are shown in Fig. 6. The saddle point of **14** (TS_{14}) is near $r_{Fe=O}$=2.04 Å and r_{FeO-C}=1.46 Å. Standard frequency analysis of **14** (TS_{14}) revealed an imaginary mode of magnitude i20.3 cm^{-1}, which indicated the expected mode along the r_{FeO-C} reaction coordinate that connects the intermediate products **16a** (IS_{16a}), **16b** (IS_{16b}), and **16c** (IS_{16c}). Although the r(Fe=O) distance of **13c** is 1.686 Å, the Fe=O bond length of **14** (TS_{14}) increases to 2.043 Å at the saddle point. The angle along the yz plane between C(5) in the thymine ring and $Fe(MeCN)_4$ plane is +149.9°, as shown in Table 2 and Fig. 6c. On the other hand, the Fe=O bond distance of **15** (TS_{15}) is 1.898 Å, which suggests that the atomic connectivity of the Fe=O double bond is stronger than that of **14** (TS_{14}).

Table 2. Parameters of Computational Geometry and Frequency in the Ground State of Optimized Transition State Thymine–O=$Fe^{IV}(AcO)(MeCN)_4^{+}$

	14 [a)] (TS_{14})	**15** [b)] (TS_{15})
r(Fe=O) (Å)	2.043	1.898
r(Fe–O^2Ac) (Å)	2.205	2.295
r(Fe–OAc) (Å)	2.213	2.169
r(Fe–N^1) (Å)	1.862	1.871
r(Fe–N^4) (Å)	1.867	1.870
r(FeO–C^5) (Å)	1.461	1.461
r(FeO–C^6) (Å)	1.461	1.472
$\angle N^1$–Fe–O^2–C^3 (°)	+155.1	−8.3
∠Fe–O–C^5 (°)	149.9	117.6
ν(FeO–thymine) cm^{-1}	i20.3	i363.4
ν(Fe–OAc) cm^{-1}	635.4	662.4
ν(FeOC=O) cm^{-1}	1681.1	1685.5
ν(Fe–OC) cm^{-1}	838.5	847.1

a, *b*) TSs (**14**, **15**) of thymine–O=$Fe^{IV}(AcO)(MeCN)_4^{+}$ in the triple spin state (M=3) and single spin state (M=1) at the UMP3(D) level, respectively. The charge (Q) is +1 in all cases. Standard thermodynamic quantities are the values at 298.15 K and 1.00 atm.

Although an imaginary **15** (TS_{15}) with a magnitude of

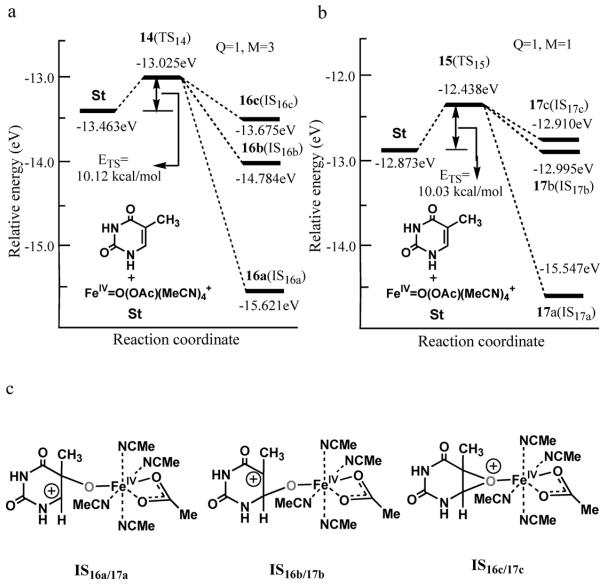

Fig. 7. Transition State and Relative Energy Profile for Oxygenation of Thymine by the $O{=}Fe^{IV}(OAc)(MeCN)_4^+$ Complex Corresponding to the (a) Triplet (M=3) and (b) Singlet (M=1) States, and (c) Three Possible Reaction Intermediates

St: starting material, thymine and $O{=}Fe^{IV}(OAc)(MeCN)_4^+$; TS: transition state; IS: intermediate state carbocation. E_{Ts} is the relative activation energy (eV) shown in the figure. The structures of $IS_{16a/17a}$, $IS_{16b/17b}$, and $IS_{16c/17c}$ are shown in Fig. 7c.

$i363.4\,cm^{-1}$ was revealed, it is caused by the vibration of Fe–OAc, and is related to the pathway whereby the AcO ligand is released from Fe. The angle along the *yz* plane between C(5) in the thymine ring and $Fe(MeCN)_4$ plane is +117.6°, as shown in Table 2 and Fig. 6f. Figures 6g and h represent the density potential surface as atomic connectivity in **14** (TS_{14}) and **15** (TS_{15}). The results support Fe–OAc of **15** (TS_{15}). Figure 7 shows the computed energy profile of the three intermediates, $IS_{16a/17a}$, $IS_{16b/17b}$, and $IS_{16c/17c}$. The relative activation energy (E_{TS}) is 10.1 kcal/mol (not including the zero point energy in molecular vibrations) as shown in Fig. 7a.

It is suggested that products **4a** and **5a** are obtained through TS along the path and the intermediate state (IS) provides **4a** and **5a** due to nucleophilic attack by CH_3COO^-. The cation intermediates **16a** (IS_{16a}), **16b** (IS_{16b}) and the cation epoxide **16c** (IS_{16c}) are formed in the triplet spin (M=3) state since in the singlet (M=1) state, they are energetically unstable (Figs. 7a, b). The C(5)–OFe bond distance in **16a** (IS_{16a}) is 1.390 Å, shorter than that of **17a** (IS_{17a}) (1.415 Å); therefore, this suggests that $O{=}Fe^{IV}(OAc)(MeCN)_4^+$ **13c** is easily released from the thymine–**13c** adduct. The reaction heat and energy profiles of the three intermediates are provided in Figs. 7a and b. The results show that the formation of **16a** (IS_{16a}) ($\Delta H = -49.8$ kcal/mol), **16b** (IS_{16b}) ($\Delta H = -30.5$ kcal/mol), and **16c** (IS_{16c}) ($\Delta H = -4.9$ kcal/mol) are exothermic processes. We demonstrated that intermediates **16a** (IS_{16a}) and **16b** (IS_{16b}) are more readily obtained than the epoxide **16c** (IS_{16c}). It is possible that the reaction producing **16a** (IS_{16a}) is promoted since the relative energy difference between **16a** (IS_{16a}) and **16b** (IS_{16b}) is about 19.3 kcal/mol.

Discussion

Thymine glycol is a product of DNA damage by reactive oxygen species and a biological marker of cancer. Important reactive oxygen species are active H_2O_2, the HO radical, HOO radical, superoxide anion radical ($O_2^{-\cdot}$), and singlet oxygen ($^1O_2$). In order to elucidate the mechanisms of oxygenation and electron removal, several Haber–Weiss–Fenton-type reactions in Fe^{2+}–H_2O_2, Fe^{3+}–EDTA–H_2O_2, Fe^{3+}–NTA–H_2O_2, and Fe^{3+}–H_2O_2–ascorbic acid systems have been used, and the oxidative damage of thymine or DNA thymine has been investigated. However, in this study, we first showed the oxygenation of thymine by a new, non-Fenton-catalyzed Haber–Weiss model: a $Fe^{II}(MeCN)_6^{2+}$–H_2O_2–Ac_2O system based on a high spin $Fe^{II}(MeCN)_6^{2+}$ complex in a hydrophobic Ac_2O–CH_3CN solution. We found that the $Fe^{II}(MeCN)_6^{2+}$–H_2O_2–Ac_2O system effectively oxidized thymine to produce the *trans*-thymine glycol derivative **4a** in good yield. Moreover, the oxygenation system produced the parabanic acid derivative **6b**, which is not produced by Fenton systems. The finding suggests that the active species of the oxygenation system differ from those of the Fenton system.

First, $Fe(MeCN)_6^{2+}$ forms a solvated molecular complex with thymine ($C_6H_6N_2O_2$) at a 1 : 1 molar ratio (Fig. 3). Next, when nucleophilic H_2O_2 is added to a dry Ac_2O–MeCN solution, the $Fe^{II}(O{-}OH)(MeCN)_n^+ \rightarrow Fe^{II}(O{-}OAc)(MeCN)_n^+$ complex produces high valency $[O{=}Fe^{IV}(OAc)(MeCN)_4]^+$ (**12** or **13**) by heterolytic –O–O– bond cleavage, as shown in Fig. 4. To determine the structure and electronic state, we used both UB3LYP/LACVP(D) and UPM3(D) methods. $O{=}Fe^{IV}(OAc)(MeCN)_4^+$ has two different active species of isomer, *cis* **9** and *trans* **10**, while *cis* **12a** is a more unstable product than *trans* **13b**. We showed that *cis* **9** is easily transformed into **11**; therefore, it is suggested that the *trans* isomer **13b** is the active species in the system. The computed energies for the active species indicate that the triple state of **13b** is more generically stable than the singlet state by 27.2 kcal/mol.

Thymine glycol derivatives, **4a**, **5a** and **5b**, produced by the oxygenation of **1a** (and **1b**) with our $Fe(MeCN)_6^{2+}$–H_2O_2–Ac_2O system, are *trans*-forms only, suggesting that the thymine glycol derivative **4a** is formed *via* the thymine epoxide or thymine cation. The thymine radical may not be an intermediate of thymine oxygenation in the $Fe^{II}(MeCN)_6^{2+}$–H_2O_2–Ac_2O system since **4a** is also formed in the presence of a radical scavenger, such as EtOH. To elucidate the mechanism of the formation of **4a**, we used the UB3LYP/LACVP(D) and UPM3(D) methods. The transition state (TS) of a triple spin state for the concerted thymine$\cdots O{=}Fe(OAc)(MeCN)_4^+$ is shown in Fig. 7. Standard frequency analysis of TS revealed the existence of a single imaginary mode with a magnitude of $i20.3\,cm^{-1}$ at the PM3(D) level. The result shows that **14** (TS_{14}) is a transition state with a low barrier, 10.1 kcal/mol. The transition state **14** (TS_{14}) formed reaction intermediates, such as thymine cation [**16a** (IS_{16a}) and **16b** (IS_{16b}) and thymine epoxide (**16c** (IS_{16c})], as shown in Figs. 6 and 7, and the connectivity of Fe=O between Fe and O is similar to that of a single bond. This suggests that the heat of formation ($\Delta H = -49.8$ kcal/mol) of **16a** (IS_{16a}) is lower than that of both **16b** (IS_{16b}) and **16c** (IS_{16c}). The reaction path determined for the oxidative dam-

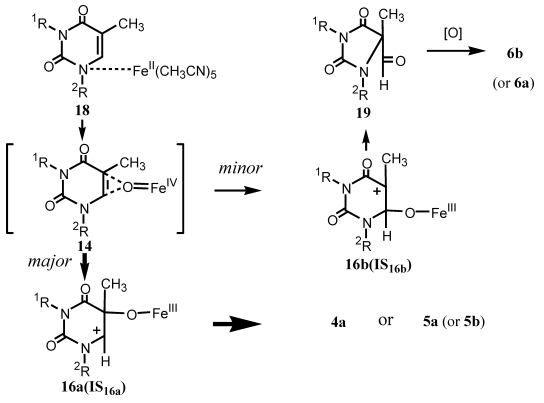

Fig. 8. Possible Path for the Oxidative Damage of Thymine in the $Fe^{II}(CH_3CN)_6^{2+}$–H_2O_2–Ac_2O System

age of thymine in the $Fe^{II}(MeCN)_6^{2+}$–H_2O_2–Ac_2O system is shown in Fig. 8. We believe that the formation of **16a** (IS_{16a}) is a major pathway in thermodynamics.

To design the activated species with high power for oxygenation, an axial ligand on the other side of the oxoiron center plane plays an important role. The high spin structure and claw-like ligand of the AcO^- active species in the oxygenation system play an important role in the production of the transition state, which is capable of strong oxygenation, as shown in Figs. 4 and 5.

Conclusion

We have reported a new model for the transformation of DNA thymine into thymine glycol with a $Fe^{II}(MeCN)_6(ClO_4)_2$–H_2O_2–Ac_2O system. The active species $O{=}Fe^{IV}(OAc)(MeCN)_4^+$ is formed under hydrophobic reaction conditions, different from the active species of a hydrophilic Fenton system. Molecular orbital stimulation revealed two types, *cis* and *trans*, of $O{=}Fe^{IV}(OAc)(MeCN)_4^+$, for AcO^- coordination on the *yz* plane. The *trans* form **13b** is more energetically stable than the *cis* form **12a**. The optimized length of $r_{Fe=O}$ between Fe and O is 1.650 Å. The formation of a high valency non-heme oxoiron ($Fe^{IV}{=}O$ or $Fe^{V}{=}O$) is possible at the hydrophobic site of the nucleus, so the oxygenation of DNA may be caused by oxygenation not only with a hydroxyl radical but also with a high valency oxoiron, because iron ions are present in nuclei in the body. Our results show that it is possible for a non-heme high valency oxoiron to form thymine glycol and parabanic acid analogues in the course of oxidative damage to thymine. Indeed, different oxidative products are observed in the reaction of thymine with the OH radical and the oxoiron $Fe^{IV}{=}O$. We therefore think that the oxygenation system and reaction mechanisms used in this study will play an important role in elucidating the oxidative damage of DNA, proteins, and drugs in antioxidant inorganic biochemistry.

Experimental

General All melting points are uncorrected. Infrared (IR) spectra were recorded with a JASCO A-100 grating spectrophotometer and UV/Vis absorption spectra were recorded using a JASCO Ubest 30 spectrophotometer. ^{1}H- and ^{13}C-NMR spectra were recorded with BRUKER AV300 or AV600 spectrometers using tetramethylsilane (TMS) as an internal standard ($CDCl_3$ solution). The mass spectra (MS) were obtained with JEOL JMS-700 or JEOL JMS-HX110 spectrometers. Thin-layer and column chromatography were performed on Merck Kieselgel 60F-254 and Wakogel C-200 silica gel (100 mesh), respectively. Elemental analyses were performed by the division of organic synthesis and analysis (located at Johoku campus), University of Ehime (Ehime, Japan).

UV/Vis Studies The concentration of [Fe^{3+}] was 1.0×10^{-4} M. Thymine MeCN solution was added to a fixed concentration (1.0×10^{-4} M) of $Fe(ClO_4)_3$ in a MeCN solution, and diluted to 10 ml with MeCN. The concentration ratios of [thymine]/[Fe^{3+}] were 0.0, 0.25, 1.0, 2.0, 3.0, and 4.0 at 305 K. Absorbance (OD) was measured at a wavelength of 340 nm.

General Procedure for Oxygenation of Thymine with $Fe(MeCN)_6(ClO_4)_2$–Ac_2O–H_2O_2 A solution of 30% H_2O_2 (2.2 ml, 20 mmol) in CH_3CN (4 ml) was added dropwise to a solution of iron(II) hexakisacetonitrile perchlorate $Fe^{II}(ClO_4)_2\cdot6H_2O$ (1.81 g, 5 mmol), Ac_2O (18 ml), and thymine (10 mmol) in MeCN (60 ml) and stirred at room temperature for 5 min. The reaction mixture was poured into water and extracted with $CHCl_3$. The combined organic layer was washed with brine, saturated with $NaHCO_3$, and water, and then dried on Na_2SO_4 and evaporated. The residue was subjected to silica gel column chromatography using $CHCl_3$–hexane (1 : 1) or $CHCl_3$ as an eluent.

Oxygenation of Thymine (1a) The reaction mixture was prepared according to the standard procedure and silica gel column chromatography of the reaction residue of thymine afforded **4a** and **2** from $CHCl_3$–hexane (1 : 1) and $CHCl_3$ as an eluent in yields of 12 and 3%, respectively.

***trans*-5,6-Dihydroxy-5,6-dehydrothymine (2)** Colorless solid; mp 221—224 °C. IR (KBr) cm^{-1}: 3400, 1670 and 1240. ^{1}H-NMR (DMSO-d_6–$CDCl_3$) δ: 1.29 (3H, s, C(5)-CH_3), 4.16 (1H, s, C(6)-H), 8.54 (1H, br, N(1)-H), and 10.16 (1H, s, N(3)-H). ^{13}C-NMR (DMSO-d_6–$CDCl_3$) δ: 23.7, 70.7, 85.0, 152.4, and 174.3. MS Calcd for $C_5H_8N_2O_4$ (M^+) *m/z*: 160.0480. Found: 160.0485.

***trans*-5,6-Diacetoxy-1-acetyl-5,6-dehydrothymine (4a)** Colorless needles, mp 131—132 °C (petroleum ether–$CHCl_3$). IR (KBr) cm^{-1}: 3240, 3120, 1760, 1720, and 1240. ^{1}H-NMR ($CDCl_3$) δ: 1.65 (3H, s, C(5)-CH_3), 2.06 (3H, s, –OCOCH$_3$), 2.10 (3H, s, –OCOCH$_3$), 2.58 (3H, s, =N–COCH$_3$), 7.43 (1H, s, C(6)-H), 7.94 (1H, br, N(3)-H). ^{13}C-NMR ($CDCl_3$) δ: 16.7, 20.5, 20.9, 26.4, 75.5, 75.5, 149.65, 165.8, 167.8, 168.8, and 170.7. MS *m/z*: Calcd for $C_{11}H_{14}N_2O_7$ (M^+): 286.0800. Found: 286.0767. UV λ_{max} (EtOH) nm (log ε): 223 (3.35).

Oxygenation of 1,3-Dimethylthymine (1b) Silica gel column chromatography of the oxygenation products of **1b** afforded **5a**, **5b**, and **6b** from the $CHCl_3$–hexane (1 : 1) and $CHCl_3$ eluates in yields of 10, 5, and 1%, respectively.

***trans*-5-Hydroxy-6-acetoxy-1,3-dimethyl-5,6-dehydrothymine (5a)** Colorless needles (hexane–ether); mp 111—113 °C. IR (KBr) cm^{-1}: 3460, 1720, 1680, and 1240. ^{1}H-NMR ($CDCl_3$) δ: 1.74 (3H, s, C(5)-CH_3), 2.20 (3H, s, –OCOCH$_3$), 3.14 (3H, s, CH_3), 3.15 (3H, s, CH_3), and 5.79 (1H, s, C(6)-H). ^{13}C-NMR ($CDCl_3$) δ: 20.9, 21.6, 28.1, 36.0, 76.5, 90.1, 151.9, 167.6, and 170.5. MS *m/z*: 230 (M^+), 213 (M^+-OH), 186 (M^+-COCH$_3$), 171 (M^+-OCOCH$_3$). MS Calcd for $C_9H_{14}N_2O_5$ (M^+) *m/z*: 230.0889. Found: 230.0907. UV λ_{max} (EtOH) nm (log ε): 236 (3.32).

***trans*-5-Acetoxy-6-hydroxy-1,3-dimethyl-5,6-dehydrothymine (5b)** Colorless oily; IR ($CHCl_3$) cm^{-1}: 3450, 1720, 1680, and 1240. ^{1}H-NMR ($CDCl_3$) δ: 1.69 (3H, s, C(5)-CH_3), 2.05 (3H, s, –OCOCH$_3$), 3.03 (3H, s, CH_3), 3.19 (3H, s, CH_3), and 5.43 (1H, s, C(6)-H). ^{13}C-NMR ($CDCl_3$) δ: 16.6, 21.5, 28.4, 33.5, 78.3, 80.9, 152.7, 167.4, and 169.8. MS *m/z*: 230 (M^+), 213 (M^+-OH), 186 (M^+-COCH$_3$).

1,3-Dimethyl Parabanic Acid (6b) Colorless plates; mp 149—151 °C ($CHCl_3$–hexane). IR (KBr) cm^{-1}: 1720. ^{1}H-NMR ($CDCl_3$) δ: 3.19 (6H, s, $CH_3\times2$). ^{13}C-NMR ($CDCl_3$) δ: 24.9, 154.1, and 159.9. *Anal.* Calcd for $C_5H_6N_2O_3$: C, 42.26; H, 4.26; N, 19.71. Found: C, 42.31; H, 4.06; N, 19.88. MS Calcd for $C_5H_6N_2O_3$ (M^+) *m/z*: 142.0379. Found: 142.0404. UV λ_{max} (EtOH) nm (log ε): 230 (3.50), 259 (2.96).

Oxygenation of Thymine in the Presence of a Radical Scavenger with $Fe(MeCN)_6(ClO_4)_2$–Ac_2O–H_2O_2 A solution of 30% H_2O_2 (2.2 ml, 20 mmol) in CH_3CN (4 ml) was slowly added dropwise to a solution of $Fe(ClO_4)_2\cdot6H_2O$ (1.81 g, 5 mmol), Ac_2O (18 ml), CH_3CH_2OH (0.46 g, 40 mmol) as a radical scavenger, and thymine (10 mmol) in CH_3CN (60 ml), and was stirred at 4 °C for 5 min.

Oxygenation of Thymine with $KMnO_4$ in Aqueous Solution *cis*-5,6-Dihydroxy-5,6-dehydrothymine (*cis*-thymineglycol) (**3**) was prepared by the method described by Benn *et al.*[23] $KMnO_4$ (1.28 g) was added to 50 ml phosphate buffer (pH=7.1) of **1a** (1.0 g) and the mixture was stirred at 18 °C for 19 h. The MnO_2 salt that precipitated was filtrated and aqueous $NaHSO_3$ was added to the filtrate, which was evaporated under reduced pressure at a temperature below 30 °C. The precipitated salt was filtrated and the filtrate with an excess of acetone was evaporated under reduced pressure. The *cis*-

thymineglycol **3** (0.23 g), colorless needles, mp 214—215 °C (lit,[23] 214—216 °C) (from aq. MeOH), was obtained.

Acetylation of 3 by DMPA-Ac_2O *cis*-Thymineglycol **3** (0.16 g, 1.02 mmol) and 20 mg DMAP were added to 20 ml of Ac_2O and the mixture was stirred for 24 h at room temperature. The resulting solution was treated with ice-water and extracted with ethyl acetate. The organic layer was washed with water, dried on Na_2SO_4, and then concentrated *in vacuo* at below 40 °C. The residue was purified by silica gel column chromatography using $CHCl_3$–hexane (2 : 1 vol%) and $CHCl_3$–hexane–AcOEt (10 : 4 : 1 vol%) as the eluent, which provided *cis*-5,6-diacetoxy-1-acetyl-5,6-dehydrothymine (**4b**) and *trans*-5,6-diacetoxy-1-acetyl-5,6-dehydro-thymine (**4a**) as colorless needles in yields of 36.7% (0.105 g) and $<$1.0%, respectively. **4b** was separated and had an *Rf* value of 0.35 ($CHCl_3$: EtOAc = 1 : 0.1). Therefore, the stereochemistry of **4a** with mp 131—132 °C and *Rf* = 0.47 ($CHCl_3$: EtOAc = 1 : 0.1) can be identified as the *trans*-form by comparison with that of **4b**.

Computational Method DFT with the B3LYP functional, which includes the Becke three-parameter exchange and the Lee, Yang, and Parr non-local correlation,[28] was used to calculate the geometry, stabilization, or activation energy (E_{TS}) of thymine carbocation, $Fe^{IV}(=O)(HOAc)(MeCN)_4^{2+} \rightarrow Fe^{III}(OH)(OAc)(MeCN)_4^{+}$, and transition state (Ts) thymine–O= $Fe(OAc)(MeCN)_4$. Geometric optimizations with a "conformer search" by the Monte-Carlo method were used at the MMFF level. Full optimization was performed with the B3LYP using LACVP(D) as a pseudopotential basis set,[29] with an effective core potential for the iron and an 6-31G(d) for C, H, O and N. All calculations used the Spartan06 and Titan programs,[30] but the optimized geometry of the transition state (Ts) thymine–O= $Fe^{IV}(OAc)(MeCN)_4^{+}$ at the saddle point was determined using the semiempirical unrestricted PM3 (UPM3(D)) method, which is suitable for transition metals. The true transition state was determined by the existence of a single mode with an imaginary frequency, followed by complete vibrational analysis.

References

1) Beckman K. B., Ames B. N., *J. Biol. Chem.*, **272**, 19633—19636 (1997).
2) Aust A. E., Eveleigh J. F., *Proc. Soc. Exp. Biol. Med.*, **222**, 246—252 (1999).
3) Valko M., Izakovic M., Mazur M., Rhodes C. J., Telser J., *Mol. Cell. Biochem.*, **266**, 37—56 (2004).
4) Cadet J., Guttin-Lombard M., Teoule R., *Int. J. Radiat. Biol. Relat. Stud. Phys. Chem. Med.*, **30**, 1—11 (1976).
5) Frelon S., Douki T., Favier A., Cadet J., *J. Chem. Soc., Perkin Trans. 1*, **2002**, 2866—2870 (2002).
6) Zhang Q., Wang Y., *J. Am. Chem. Soc.*, **126**, 13287—13297 (2004).
7) Aruoma O. I., Halliwell B., *Chem. Br.*, **27**, 149—152 (1991).
8) Koppenol W. H., *Redox Rep.*, **6**, 229—234 (2001).
9) Harayama T., Kotoji K., Yanada R., Yoneda F., Taga T., Osaki K., Tomohisa H., *Chem. Pharm. Bull.*, **34**, 2354—2361 (1986).
10) Henle E. S., Han Z., Tang N., Rai P., Luo Y., Linn S., *J. Biol. Chem.*, **274**, 962—971 (1999).
11) Umemura T., Sai K., Takagi A., Hasegawa R., Kurokawa Y., *Carcinogenesis*, **11**, 345—347 (1990).
12) Kasai H., Nishimura S., *Nucleic Acids Res.*, **12**, 2137—2147 (1984).
13) Miller H., Fernandes A. S., Zaika E., McTigue M. M., Torres M. C., Wente M., Iden C. R., Grollman A. P., *Nucleic Acids Res.*, **32**, 338—345 (2004).
14) Stephenson N. A., Bell A. T., *Inorg. Chem.*, **45**, 2278—2285 (2007).
15) Groves J. T., *J. Inorg. Biochem.*, **100**, 434—447 (2006).
16) Cathcart R., Schwiers E., Soul R. L.,Ames B. N., *Proc. Natl. Acad. Sci. U.S.A.*, **81**, 5633—5637 (1984).
17) Miller H., Fernandes A. S., Zaika E., McTigue M. M., Torres M. C., Wente M., Iden C. R., Grollman A. P., *Nucleic Acids Res.*, **32**, 338—345 (2004).
18) Takao K., Kanno S., Shiromoto T., Hasegawa R., Ide H., Ikeda S., Sarker A. H., Seki S., Xing J. Z., Le X. C., Weinfeld M., Kobayashi K., Miyazaki J., Muijtjens M., Hoeijmakers J. H., van der Horst H. G., Yasui A., Sarker A. H., *EMBO J.*, **21**, 3486—3493 (2002).
19) Kotani E., Kobayashi S., Ishii Y., Tobinaga S., *Chem. Pharm. Bull.*, **32**, 4281—4291 (1984).
20) Kotani E., Kobayashi S., Ishii Y., Tobinaga S., *Chem. Pharm. Bull.*, **33**, 4671—4679 (1985).
21) Kobayashi S., Kotani E., Ishii Y., Tobinaga S., *Chem. Pharm. Bull.*, **37**, 610—614 (1989).
22) Kotani E., *Yakugaku Zasshi*, **124**, 873—892 (2004).
23) Benn M. H., Chatamra B., Jones A. S., *J. Chem. Soc.*, **1960**, 1014—1020 (1960).
24) Iida S., Hayatsu H., *Biochem. Biophys. Acta*, **213**, 1—13 (1970).
25) Itahara T., Fujii Y., Tada M., *J. Org. Chem.*, **53**, 3421—3424 (1988).
26) Stoyanov S. R., Villegas J. M., Rillema D. P., *Inorg. Chem.*, **41**, 2941—2945 (2002).
27) Howell J. O., Goncalves J. M., Amatore C., Klasinc L., Wightman R. M., Kochi J. K., *J. Am. Chem. Soc.*, **106**, 3968—3976 (1984).
28) Hay P. J., Wadt W. R., *J. Chem. Phys.*, **82**, 299—310 (1985).
29) Rohde J.-U., Torelli S., Shan X., Lim M. H., Klinker E. J., Kaizer J., Chen K., Nam W., Que L. Jr., *J. Am. Chem. Soc.*, **126**, 16750—16761 (2004).
30) Titan and Spartan06, Wavefunction, Inc., Irvine, CA, U.S.A.